

Refined Gradient-Based Temperature Optimization for the Replica-Exchange Monte-Carlo Method

Tatsuya Miyata, Shunta Arai, and Satoshi Takabe
Institute of Science Tokyo, Okayama, Tokyo 152-8550, Japan
(Dated: January 21, 2026)

The replica-exchange Monte-Carlo (RXMC) method is a powerful Markov-chain Monte-Carlo algorithm for sampling from multi-modal distributions, which are challenging for conventional methods. The sampling efficiency of the RXMC method depends highly on the selection of the temperatures, and finding optimal temperatures remains a challenge. In this study, we propose a refined online temperature selection method by extending the gradient-based optimization framework proposed previously. Building upon the existing temperature update approach, we introduce a reparameterization technique to strictly enforce physical constraints, such as the monotonic ordering of inverse temperatures, which were not explicitly addressed in the original formulation. The proposed method defines the variance of acceptance rates between adjacent replicas as a loss function, estimates its gradient using differential information from the sampling process, and optimizes the temperatures via gradient descent. We demonstrate the effectiveness of our method through experiments on benchmark spin systems, including the two-dimensional ferromagnetic Ising model, the two-dimensional ferromagnetic XY model, and the three-dimensional Edwards-Anderson model. Our results show that the method successfully achieves uniform acceptance rates and reduces round-trip times across the temperature space. Furthermore, our proposed method offers a significant advantage over recently proposed policy gradient method that require careful hyperparameter tuning, while simultaneously preventing the constraint violations that destabilize optimization.

I. INTRODUCTION

Markov-chain Monte-Carlo (MCMC) methods [1, 2] are powerful algorithms used to sample from complex probability distributions that are often intractable to sample from directly. However, these conventional MCMC methods often face difficulties when sampling from multi-modal distributions, particularly the Boltzmann distributions of systems with rugged energy landscapes. In such systems, the Markov chain can become trapped in local energy minima, leading to insufficient exploration of the state space and significantly slow relaxation times.

To overcome this problem, the replica-exchange Monte-Carlo (RXMC) method [3–5], also known as parallel tempering, was proposed. This method simultaneously simulates multiple auxiliary chains, known as replicas, at different temperatures and periodically exchanges their states between adjacent replicas according to an acceptance rate that satisfies the detailed balance condition. While high-temperature replicas can easily overcome entropic barriers by exploring a flattened energy landscape, low-temperature replicas perform precise local exploration. This exchange mechanism allows low-temperature replicas to efficiently transition to new modes that would otherwise be difficult to reach on their own, making it a powerful tool used in a wide range of fields, including the study of spin glasses [3, 4] and protein folding problems [6].

However, the performance of RXMC depends critically on the choice of the temperatures. Poorly chosen temperatures can lead to bottleneck where the acceptance rate between adjacent replicas drops significantly, hindering the random walk in temperature space. While simple

heuristic strategies such as arranging temperatures in a geometric progression [7] are widely used, they rely on specific assumptions like constant specific heat. These assumptions usually break down in systems exhibiting phase transitions. Consequently, establishing a strategy to automatically determine the optimal temperatures for a given target system remains an open problem.

To address this problem, various temperature selection methods have been proposed. Common strategies aim for uniform acceptance rates across all adjacent pairs [3, 6, 8–13] or minimizing the round-trip time, that is, maximizing the round-trip rate [14–17]. Other approaches employ specific physical metrics, such as maximizing the mean squared displacement [18, 19] or uniformizing the Kullback-Leibler divergence between the Boltzmann distributions of adjacent replicas [12]. However, these conventional strategies often face practical challenges. Many of these require computationally expensive preliminary runs for offline optimization or involve complex hyperparameter tuning that depends on the system’s specific properties. These limitations highlight the need for a more versatile and automated approach that can dynamically optimize the temperatures during the simulation without extensive manual intervention.

Recently, gradient-based online optimization methods have emerged as a promising alternative. These approaches define a differentiable loss function representing sampling efficiency and optimize the inverse temperature vector $\beta = (\beta_1, \beta_2, \dots, \beta_M)$ via gradient ascent or gradient descent during the simulation, where M is the number of replicas. A significant advantage of these methods is their high extensibility and versatility; they allow for the selection of any differentiable metric as the loss function and enable automatic optimization of the tem-

perature vector without requiring prior knowledge of a model. One approach calculates the gradient of the loss function directly using sampling data [20]. While this direct method avoids the complexity of policies, the original formulation does not explicitly enforce the monotonic constraints inherent to the inverse temperature vector, namely that $\beta_1 < \beta_2 < \dots < \beta_M$. This oversight often leads to constraint violations and destabilizes the optimization process, as will be demonstrated later. Another adaptive approach employs the policy gradient method from reinforcement learning [21]. It employs a parameterized policy to simplify the update rules. However, this parameterization restricts the flexibility of the inverse temperature vector and necessitates tedious tuning of hyperparameters. Furthermore, the effectiveness of these gradient-based methods has primarily been demonstrated on continuous systems, and their applicability to discrete spin systems with phase transitions remains unverified.

Therefore, this study aims to develop a refined online temperature selection strategy by extending the gradient-based optimization framework proposed previously [20]. While adopting their temperature update approach, we introduce a reparameterization technique to address monotonicity constraints that were not explicitly enforced in their original formulation. Our contributions are summarized as follows:

- 1) We refine the optimization framework in [20] to strictly guarantee the satisfaction of constraints inherent to the temperature vector, specifically the monotonic ordering of inverse temperatures. By incorporating these constraints directly via a variable transformation, our approach mathematically guarantees the satisfaction of these constraints during the optimization while retaining the advantage of avoiding complex policy hyperparameter tuning.
- 2) We demonstrate the effectiveness of the proposed method on spin systems exhibiting phase transitions, where the applicability of conventional gradient-based methods remains unclear. Specifically, we apply it to the Ising model, the XY model, and the Edwards-Anderson model, showing that it can successfully achieve uniform acceptance rates between adjacent replicas.

The remainder of this paper is organized as follows. Section II reviews related work, and Section III details our proposed method. Section IV presents the experimental setup, results, and discussion. Finally, Section V concludes the paper.

II. RELATED WORK

This section reviews key concepts and prior work relevant to our proposed method. We first provide a brief overview of the RXMC method itself. Then, we introduce the round-trip time, a crucial metric for evaluating its efficiency. Finally, we discuss recent approaches using

policy gradient methods for temperature optimization, highlighting their strengths and limitations.

A. Replica-exchange Monte-Carlo

In the RXMC method, M non-interacting copies of the system of interest, called replicas, are simulated simultaneously using a vector of M inverse temperatures $\beta = (\beta_1, \beta_2, \dots, \beta_M)$. These inverse temperatures span a wide range and are ordered monotonically such that $\beta_1 < \beta_2 < \dots < \beta_M$. The lowest inverse temperature β_1 is set small enough to allow the system to easily overcome large energy barriers, while the highest inverse temperature β_M is set large enough to ensure detailed sampling of local energy minima. The RXMC method consists of two alternating processes. The first is the intra-replica update. In this phase, each of the M replicas evolves independently for a specified number of Monte-Carlo steps (MCS). The evolution follows a standard MCMC procedure, such as the Metropolis-Hastings algorithm [2], according to the target distribution at that replica's assigned inverse temperature. This allows each replica to explore the state space locally and equilibrate within its own canonical ensemble. The second is the inter-replica exchange, which characterizes this method. Following the intra-replica update, exchanges are attempted between replicas at adjacent inverse temperatures. For a pair of replicas at neighboring inverse temperatures β_i and β_{i+1} ($i = 1, \dots, M - 1$), a proposal is made to swap their states. This proposed swap is accepted with probability based on the detailed balance condition for the extended ensemble. The acceptance rate between adjacent replicas is defined by the Metropolis criterion:

$$A_{i,i+1}(\beta_i, \beta_{i+1}) = \min \{1, \exp(\Delta\beta\Delta E)\}, \quad (1)$$

where $\Delta\beta = \beta_{i+1} - \beta_i$ is the difference between the inverse temperatures and $\Delta E = E_{i+1} - E_i$ is the energy difference between the states of the two replicas.

The advantage of RXMC stems from this exchange mechanism. Conventional MCMC methods based on local update often become trapped in local minima separated by energy barriers. In contrast, the swap moves in RXMC induce a random walk in temperature space, enabling replicas to overcome these energy barriers and escape local minima by traversing to high temperatures where equilibration is rapid and subsequently returning to low temperatures. This effective thermal tunneling across energy barriers accelerates the global exploration of the system's energy landscape and significantly reduces relaxation times.

The efficiency of this exchange process relies heavily on the choice of the inverse temperature vector. For the random walk to proceed smoothly, there must be sufficient overlap between the Boltzmann distributions of adjacent replicas to ensure non-vanishing acceptance rates. A widely used heuristic for determining this placement

is the geometric progression [7], which arranges temperatures according to the following equation:

$$\beta_j = \beta_M \left(\frac{\beta_1}{\beta_M} \right)^{\frac{M-j}{M-1}} \quad (j = 1, 2, \dots, M). \quad (2)$$

This strategy is characterized by having denser temperature intervals in the low-temperature region where relaxation is assumed to be slower. It can achieve uniform acceptance rates between adjacent replicas provided that the system's specific heat is constant regardless of temperature [13]. However, the assumption of constant specific heat does not hold for general systems, especially those exhibiting phase transitions. As a result, the acceptance rates become unbalanced, leading to bottlenecks where exploration stagnates in a certain temperature range. To address this issue, various heuristic methods have been developed to determine system-dependent temperatures, as reviewed in the previous section.

B. Round-trip Time

A key metric for evaluating the overall sampling efficiency of the RXMC method is the round-trip time τ_{RT} . This represents the MCS required for a single replica to travel back and forth between the lowest and highest inverse temperatures.

This total time is conceptually divided into two parts. Consider a replica starting at the highest inverse temperature β_M . The first part, τ_{down} is the time taken for this replica to perform a random walk in the inverse temperature space and reach the lowest inverse temperature β_1 for the first time. The second part, τ_{up} is the subsequent time taken for the replica to return to β_M for the first time. The total round-trip time is thus defined as $\tau_{\text{RT}} = \tau_{\text{down}} + \tau_{\text{up}}$. A shorter τ_{RT} indicates a more efficient traversal of the inverse temperature space and, consequently, better exploration of the state space.

To measure these times in a simulation, a labeling scheme can be employed [14]. Each replica can be assigned a label indicating its direction of travel in the temperature space. For instance, a replica at β_M might start with a label “down”. This label remains until the replica reaches the opposite extreme, β_1 , for the first time, at which point its label changes to “up”. Similarly, an “up” replica changes its label back to “down” only upon its first return visit to β_M . By recording the time intervals between these label changes, one can measure τ_{down} and τ_{up} , and consequently the round-trip time τ_{RT} .

C. Policy Gradient Method for Temperature Selection

Recently, the selection problem of the optimal temperatures in the RXMC method has been modeled as a single-state reinforcement learning problem by Zhao and

Pillai, applying policy gradient methods [21]. In this context, a single-state problem implies that the environment does not transition between different states based on the agent's actions.

In their approach, an action \mathbf{a} representing the temperatures was sampled from a parameterized stochastic policy $\pi_{\boldsymbol{\theta}}$, and the policy parameters $\boldsymbol{\theta}$ were updated based on a reward quantifying the sampling efficiency.

The objective in policy gradient methods is to find the optimal parameters $\boldsymbol{\theta}$ that maximize the expected reward $J(\boldsymbol{\theta}) := \mathbb{E}_{\pi_{\boldsymbol{\theta}}}[R_{\mathbf{a}}]$, where $R_{\mathbf{a}}$ is the reward obtained for the action \mathbf{a} . The parameters are optimized via gradient ascent:

$$\boldsymbol{\theta} \leftarrow \boldsymbol{\theta} + \eta(J(\boldsymbol{\theta}) - \bar{R}) \nabla_{\boldsymbol{\theta}} \log \pi_{\boldsymbol{\theta}}(\mathbf{a}), \quad (3)$$

where η is the learning rate, and \bar{R} is a reward baseline used to reduce the variance of the gradient estimate. Algorithm 1 outlines the policy gradient method in the single-state case.

Algorithm 1 Single-State Policy Gradient [21]

Input: policy distribution $\pi_{\boldsymbol{\theta}}(\cdot)$, learning rate η , epochs T
Initialize: policy parameters $\boldsymbol{\theta}_0$, MCMC states $\{\mathbf{x}_0^{(i)}\}_{i=1}^M$
1: **for** $t = 0, 1, \dots, T-1$ **do**
2: Generate a vector of sampler parameters \mathbf{a}_t by drawing from the policy distribution $\pi_{\boldsymbol{\theta}_t}$.
3: Run RXMC sampler with parameters \mathbf{a}_t and observe the reward r_t .
4: Update the average reward \bar{R} based on observed rewards.
5: Calculate the gradient of policy $g_t = \nabla_{\boldsymbol{\theta}} \log \pi_{\boldsymbol{\theta}}(\mathbf{a}_t) |_{\boldsymbol{\theta}=\boldsymbol{\theta}_t}$ w.r.t. $\boldsymbol{\theta}$ and clip it.
6: Update the policy parameters: $\boldsymbol{\theta}_{t+1} = \boldsymbol{\theta}_t + \eta(r_t - \bar{R})g_t$.
7: **end for**
Output: Final optimized policy parameters $\boldsymbol{\theta}_T$.

Specifically, the action space was defined using the differences of logarithmic inverse temperatures $D_i = \log \beta_{i+1} - \log \beta_i$, resulting in $\mathbf{a} = (D_1, \dots, D_{M-1}) \in [0, \infty)^{M-1}$. Using the differences of logarithmic inverse temperatures ensures that the scale of all parameters is similar, which contributes to learning stability and allows for easily fixing the boundary conditions. Additionally, a multivariate Gaussian distribution with mean $\boldsymbol{\theta}$ and variance-covariance matrix $\sigma^2 \mathbf{I}$ was used as the policy distribution, where \mathbf{I} denotes the identity matrix. The primary rationale for this choice is the analytical simplicity of the gradient computation. Regardless of the complexity of the target system, this formulation reduces the gradient of the log-policy to a simple form:

$$\nabla_{\boldsymbol{\theta}} \log \pi_{\boldsymbol{\theta}}(\mathbf{a}_t) = \frac{\mathbf{a}_t - \boldsymbol{\theta}}{\sigma^2}. \quad (4)$$

However, the experiments conducted in [21] were only on continuous distributions, such as the multi-modal Gaussian distribution and Boltzmann distributions with

Rosenbrock and egg-box functions. Thus, the applicability of their method to discrete variable systems, particularly spin systems like the Ising model, remains unveiled. Specifically, in systems exhibiting phase transitions, the assumption that the differences of logarithmic inverse temperatures share a similar scale may be violated due to the significant variations in required temperature intervals. This discrepancy could destabilize the learning process, necessitating a rigorous verification in these contexts. Furthermore, the method requires setting several hyperparameters such as the initial policy parameters θ_0 , the policy variance σ^2 , and the learning rate η . The tuning process can be complex and tedious. In particular, the policy variance σ^2 is critical to the convergence of the policy gradient method, and the method may fail to converge if they are not tuned appropriately.

III. TEMPERATURE OPTIMIZATION

In this study, we propose a refined framework to optimize the inverse temperatures in the RXMC method. The core idea is to iteratively update the inverse temperature vector β to minimize a predefined loss function $f(\beta)$ that quantifies sampling efficiency. This optimization is performed using a gradient-based approach. A key feature of our framework is that the gradient of the loss function is estimated directly by utilizing observables obtained from the sampling process itself.

A. Loss Function

Our primary objective is to achieve uniform acceptance rates between adjacent replicas. This heuristic goal is motivated by the physical intuition that any local suppression of acceptance rates acts as a bottleneck, impeding the random walk of replicas in the temperature space. Eliminating such bottlenecks to ensure smooth flow of replicas is expected to lead to faster relaxation. This goal of uniformity can be mathematically formulated as a minimization problem. Accordingly, we define the loss function as the variance of the expected acceptance rates across all adjacent replica pairs:

$$f_{\text{uni}}(\beta) = \frac{1}{M-1} \sum_{i=1}^{M-1} (\mathbb{E}[A_{i,i+1}(\beta_i, \beta_{i+1})] - \bar{A})^2, \quad (5)$$

where $A_{i,i+1}$ is the acceptance rate between adjacent replicas at inverse temperatures β_i and β_{i+1} as defined in Eq. (1) and $\bar{A} = \sum_{i=1}^{M-1} \mathbb{E}[A_{i,i+1}]/(M-1)$. We optimize the inverse temperature vector β that minimizes this loss function.

As an alternative approach for gradient-based optimization, MacCallum *et al.* proposed a metric that maximizes the product of acceptance rates to avoid bottlenecks in the random walk [20]. To apply gradient descent,

we reformulate the objective as the sum of the negative natural logarithms of the expected acceptance rates:

$$f_{\log}(\beta) = - \sum_{i=1}^{M-1} \log(\mathbb{E}[A_{i,i+1}(\beta_i, \beta_{i+1})]). \quad (6)$$

Minimizing this function heavily penalizes small acceptance rates due to the logarithmic singularity near zero, thereby naturally encouraging the elimination of bottlenecks. In this study, we also assess the effectiveness of this logarithmic metric on the Ising model, and compare it with the variance of the expected acceptance rates. We directly utilize the gradient derivation provided in their work for the optimization.

While other metrics, such as the round-trip time or the integrated autocorrelation time, could be used as the loss function, they are not practical for online optimization. Estimating these quantities accurately requires large MCS, making them computationally expensive to evaluate at each step of an iterative optimization process. Estimates from short runs, on the other hand, suffer from large statistical variance, which would make the learning process unstable. Therefore, we adopt the variance of acceptance rates as a computationally feasible and effective proxy for improving overall sampling efficiency.

B. Gradient Estimation via the Score Function Method

To minimize the loss function $f_{\text{uni}}(\beta)$ defined in the previous section, we employ gradient descent. In this study, the minimum and maximum inverse temperatures β_1 and β_M are fixed to ensure the inverse temperatures span the desired regimes. Consequently, the optimization targets the intermediate inverse temperatures from β_2 to β_{M-1} .

A straight-forward approach is to treat the inverse temperature vector β directly as the parameters and compute its gradient $\nabla_{\beta} f_{\text{uni}}$. However, it is suggested that direct optimization in this parameter space can be unstable and prone to trapping in undesirable local minima [20]. Indeed, in our preliminary experiments described in Appendix A, we observed that directly updating β often resulted in the stagnation of the optimization process. The instability is primarily attributed to the characteristics of the gradient. In the initial phase of optimization, the inverse temperatures tend to drift away from critical regions, leading to excessive intervals between adjacent replicas. Consequently, the acceptance rate associated with these excessive intervals drop to nearly zero. In this regime, the optimization process loses the effective driving force to correct the intervals, leading to stagnation. While employing a larger learning rate could help the system escape such stagnation, it inevitably leads to a violation of the monotonicity constraint $\beta_1 < \beta_2 < \dots < \beta_M$, as the update magnitude can easily exceed the interval between neighbors.

To circumvent these issues, we introduce a reparameterization of the variables. We adopt the logarithm of the inverse temperature differences as the optimization parameters. Specifically, we define the parameter vector $\mathbf{L} = (L_1, \dots, L_{M-2})$, where each element corresponds to the log-difference $L_k = \log \Delta\beta_k = \log(\beta_{k+1} - \beta_k)$ for $k = 1, \dots, M-2$. Although there are $M-1$ intervals in total, the constraint of fixed endpoints imposes the condition $\sum_{k=1}^{M-1} \Delta\beta_k = \beta_M - \beta_1$. This constraint reduces the degrees of freedom by one, leaving $M-2$ independent variables to be optimized. This formulation allows for flexible exploration of the parameter space while strictly maintaining the order of temperatures.

The partial derivative of the loss function f_{uni} with respect to the parameter L_k is derived using the chain rule as follows:

$$\begin{aligned} \frac{\partial f_{\text{uni}}}{\partial L_k} &= \sum_{j=2}^{M-1} \frac{\partial f_{\text{uni}}}{\partial \beta_j} \frac{\partial \beta_j}{\partial L_k} \\ &= \sum_{j=2}^{M-1} \sum_{n=1}^{M-2} \frac{\partial f_{\text{uni}}}{\partial \beta_j} \frac{\partial \beta_j}{\partial \Delta\beta_n} \frac{\partial \Delta\beta_n}{\partial L_k} \\ &= \Delta\beta_k \sum_{j=2}^{M-1} \sum_{n=1}^{M-2} \frac{\partial f_{\text{uni}}}{\partial \beta_j} \frac{\partial \beta_j}{\partial \Delta\beta_n}. \end{aligned} \quad (7)$$

First, we compute the partial derivative of the loss function with respect to an arbitrary intermediate inverse temperature β_j ($j = 2, \dots, M-1$). Considering that β_j only affects the acceptance rates $A_{j-1,j}$ and $A_{j,j+1}$ of the adjacent pairs, the derivative is given by:

$$\begin{aligned} \frac{\partial f_{\text{uni}}}{\partial \beta_j} &= \frac{2}{M-1} \left\{ (\mathbb{E}[A_{j-1,j}] - \bar{A}) \frac{\partial}{\partial \beta_j} \mathbb{E}[A_{j-1,j}] \right. \\ &\quad \left. + (\mathbb{E}[A_{j,j+1}] - \bar{A}) \frac{\partial}{\partial \beta_j} \mathbb{E}[A_{j,j+1}] \right\}, \end{aligned} \quad (8)$$

where $\mathbb{E}[\cdot]$ denotes the expectation taken with respect to the joint distribution of the relevant replicas. Specifically, the term $\mathbb{E}[A_{j-1,j}]$ represents the expectation over the product of the independent probability distributions at inverse temperatures β_{j-1} and β_j .

This expression contains the gradients of the expected acceptance rates, which generally cannot be computed directly. To estimate these terms, we employ the score function method [22]. This technique, also known as the log-derivative trick, allows the gradient of an expectation to be expressed as an expectation involving the gradient of the log-probability, without requiring differentiation of the function inside the expectation:

$$\nabla_{\boldsymbol{\theta}} \mathbb{E}[f(X(\boldsymbol{\theta}))] = \mathbb{E}[f(X) \nabla_{\boldsymbol{\theta}} \log p(X|\boldsymbol{\theta})]. \quad (9)$$

We note that stochastic automatic differentiation (StochasticAD) [23, 24] serves as an alternative method for estimating such gradients, which is briefly discussed in Appendix B.

Applying the score function method, the term $\partial \mathbb{E}[A_{j-1,j}] / \partial \beta_j$ is calculated as:

$$\frac{\partial \mathbb{E}[A_{j-1,j}]}{\partial \beta_j} = \mathbb{E} \left[\frac{\partial A_{j-1,j}}{\partial \beta_j} + A_{j-1,j} \frac{\partial}{\partial \beta_j} \log p(\boldsymbol{\sigma}; \beta_j) \right]. \quad (10)$$

Here, $p(\boldsymbol{\sigma}; \beta_j)$ is the probability distribution at inverse temperatures β_j . Considering the Boltzmann distribution, $p(\boldsymbol{\sigma}; \beta) \propto \exp(-\beta H(\boldsymbol{\sigma}))$, the derivative of the log-probability becomes:

$$\frac{\partial}{\partial \beta_j} \log p(\boldsymbol{\sigma}; \beta_j) = \langle H \rangle_{\beta_j} - H(\boldsymbol{\sigma}), \quad (11)$$

where $H(\boldsymbol{\sigma})$ is the energy of state $\boldsymbol{\sigma}$, and $\langle H \rangle_{\beta_j}$ is the expectation of the energy at inverse temperature β_j . Consequently, the gradient $\partial \mathbb{E}[A_{j-1,j}] / \partial \beta_j$ can be written analytically as [20, 25]:

$$\frac{\partial \mathbb{E}[A_{j-1,j}]}{\partial \beta_j} = \langle H \rangle_{\beta_j} \mathbb{E}[A_{j-1,j}] - \mathbb{E}[H A_{j-1,j}]. \quad (12)$$

The term $\partial \mathbb{E}[A_{j,j+1}] / \partial \beta_j$ is obtained through a similar calculation.

Next, we evaluate the partial derivative of β_j with respect to $\Delta\beta_n$. Since β_j is expressed as $\beta_j = \beta_1 + \sum_{n=1}^{j-1} \Delta\beta_n$, we have:

$$\frac{\partial \beta_j}{\partial \Delta\beta_n} = \begin{cases} 1 & (n < j), \\ 0 & (n \geq j). \end{cases} \quad (13)$$

Substituting these results into Eq. (7), the gradient of the loss function with respect to L_k is derived as:

$$\frac{\partial f_{\text{uni}}}{\partial L_k} = \Delta\beta_k \sum_{j=k+1}^{M-1} \frac{\partial f_{\text{uni}}}{\partial \beta_j} \quad (k = 1, \dots, M-2). \quad (14)$$

This formula consists entirely of observables estimated by the RXMC simulation. Due to the constraints fixing the endpoints β_1 and β_M , determining $M-2$ elements of \mathbf{L} automatically fixes the remaining interval. Thus, $\Delta\beta_{M-1}$ is determined by:

$$\Delta\beta_{M-1} = \beta_M - \beta_1 - \sum_{k=1}^{M-2} \Delta\beta_k. \quad (15)$$

This formulation allows us to estimate the gradient directly from sampling data and iteratively update the parameter set \mathbf{L} using the following update rule:

$$\mathbf{L} \leftarrow \mathbf{L} - \eta \nabla_{\mathbf{L}} f_{\text{uni}}(\boldsymbol{\beta}), \quad (16)$$

where η is the learning rate. Algorithm 2 summarizes the proposed iterative procedure based on this update rule.

Algorithm 2 Gradient Descent via Score Function Method

Input: learning rate η , epochs T , batch size B
Initialize: inverse temperature vector $\beta^{(0)} = (\beta_1^{(0)}, \dots, \beta_M^{(0)})$,
MCMC states $\{\sigma_0^{(i)}\}_{i=1}^M$

- 1: **for** $t = 0, 1, \dots, T - 1$ **do**
- 2: Initialize gradient estimate $\mathbf{g}^{(t)} = \mathbf{0}$
- 3: **for** $b = 1, \dots, B$ **do**
- 4: Run an independent RXMC simulation with parameters $\beta^{(t)}$.
- 5: Estimate stochastic gradient $\nabla_{\mathbf{L}} f_{\text{uni}}(\beta)|_{\beta=\beta^{(t)}}$ from this b -th simulation.
- 6: $\mathbf{g}^{(t)} \leftarrow \mathbf{g}^{(t)} + \nabla_{\mathbf{L}} f_{\text{uni}}(\beta)|_{\beta=\beta^{(t)}}$
- 7: **end for**
- 8: $\mathbf{g}^{(t)} \leftarrow \mathbf{g}^{(t)}/B$
- 9: Update the parameters via stochastic gradient descent:
- 10: $\mathbf{L}^{(t+1)} \leftarrow \mathbf{L}^{(t)} - \eta \mathbf{g}^{(t)}$
- 11: Update $\beta^{(t+1)}$ from $\mathbf{L}^{(t+1)}$ ensuring boundary constraints.
- 12: **end for**

Output: Optimized inverse temperature vector $\beta^{(T)}$.

Algorithm 2 employs a batch learning approach. The gradient $\nabla_{\mathbf{L}} f_{\text{uni}}(\beta)$ is estimated as an average over a mini-batch of B independent RXMC simulations at each epoch t . A gradient estimated from a single simulation where $B = 1$ can have high variance due to the stochastic nature of the MCMC process. By averaging over a batch, we obtain a more stable gradient estimate, which helps to stabilize the learning process and improves convergence.

IV. NUMERICAL SIMULATIONS

In this section, we describe the numerical experiments conducted to validate our proposed optimization method. We first detail the general experimental setup common to all models. Then, we present the results for three benchmark models: the two-dimensional (2D) ferromagnetic Ising model, the 2D ferromagnetic XY model, and the 3D Edwards-Anderson spin-glass model.

A. Setup

We detail the common settings used throughout the following simulations. The RXMC method involves two alternating processes: local updates and replica exchanges. For the local updates, we employed the standard Metropolis-Hastings algorithm [1, 2] with single-spin flip dynamics. Following each MCS of local updates, exchange attempts are performed between adjacent replicas. Specifically, we adopted the standard alternating schedule [3], where exchanges between odd-indexed pairs and even-indexed pairs are attempted alternately at every MCS.

As the initial values for the optimization of the inverse temperature vector, we used the geometric progression defined in Eq. (2). The specific values for the lowest

inverse temperature β_1 and the highest inverse temperature β_M are set individually for each target model to sufficiently cover the temperature range of interest, particularly including any critical regions.

In addition to the inverse temperatures, the total number of replicas M is also a crucial parameter. While optimizing M to balance the overlap between the Boltzmann distributions of adjacent replicas and computational cost is a critical topic [14, 26], our proposed method focuses on optimizing the placement of inverse temperatures for a given fixed M . Therefore, the total number of replicas M was fixed at $M = 20$ for all simulations in this study. The determination of the optimal M is left for future work.

We adopted the variance of the acceptance rates between the adjacent replicas, defined in Sec. III A, as the loss function for the optimization. To estimate the gradient of this loss function, each independent simulation within a batch consists of an equilibration phase of N_{eq} MCS followed by a sampling phase of N_{sam} MCS. The duration N_{eq} is chosen to allow the system to reach thermal equilibrium. The sampling duration N_{sam} is set to a length sufficient to suppress the statistical variance of the estimated gradient, thereby ensuring stable learning updates. Specific values for N_{eq} and N_{sam} are provided in the respective subsections for each model.

Parameter updates were performed using the Adam optimizer [27] with stochastic gradients estimated from the loss function. The hyperparameters were set as follows: learning rate $\eta = 0.005$, epochs $T = 300$, and batch size $B = 10$.

As a metric to evaluate the sampling efficiency of the optimized inverse temperatures, we measured the round-trip time. For comparison, we also measured the round-trip times for two conventional strategies: a geometric progression as defined in Eq. (2) and a linearly spaced inverse temperatures defined as:

$$\beta_j = \beta_1 + (\beta_M - \beta_1) \frac{j-1}{M-1} \quad (j = 1, 2, \dots, M). \quad (17)$$

Hereafter, we refer to this strategy as “inverse linear”.

The round-trip times of the proposed and baseline methods were evaluated by 10^7 MCS for each of the final optimized vector and the two comparison strategies. The distribution of round-trip times observed during these simulations was recorded, and the results were visualized using box plots.

B. Ising Model

To verify the proposed method, we start with the 2D ferromagnetic Ising model, which is the simplest spin system. The Hamiltonian $\mathcal{H}_{\text{Ising}}$ of this model is given by:

$$\mathcal{H}_{\text{Ising}} = -J \sum_{\langle i,j \rangle} \sigma_i \sigma_j, \quad (18)$$

where $\sigma_i \in \{\pm 1\}$ represents the Ising spins on a square lattice with $N = L^2$ total spins ($i = 1, \dots, N$). The summation $\sum_{\langle i,j \rangle}$ denotes the sum over all pairs of nearest-neighbor spins. The constant J determines the strength of the interaction between spins, and in this study, we set $J = 1$ to consider ferromagnetic interactions. The 2D Ising model is known to exhibit a phase transition from an ordered phase to a disordered phase at a finite temperature. Near the critical point, the specific heat diverges and energy fluctuations become maximal. Therefore, this temperature region tends to become a sampling bottleneck in the RXMC method, making the optimization of the temperatures particularly important.

In the simulation, we used a system with a side length of $L = 20$ and imposed periodic boundary conditions to suppress finite-size effects. The hyperparameters of the initial inverse temperature vector, the geometric progression, were set to $\beta_1 = 0.1, \beta_M = 1.0$ chosen to fully include the critical region. Furthermore, we set the number of equilibration steps to $N_{\text{eq}} = 10^2$ MCS and the sampling steps to $N_{\text{sam}} = 10^4$ MCS.

For comparison, we also present the results obtained using the policy gradient method, which was described in Sec. II C. The following settings were used: the initial temperature vector was the geometric progression, and the initial policy parameter θ was obtained by transforming this initial vector into the differences of logarithmic inverse temperatures. The standard deviation of the policy distribution was set as:

$$\sigma(t) = \frac{0.05}{(\eta + 1)^t}, \quad (19)$$

where η is the learning rate and t is the epoch. This annealing schedule was applied to accelerate convergence. Considering that the policy is maximized via gradient ascent, we adopted the negative of the variance of acceptance rates between adjacent replicas as the reward function. The optimizer was the same as that used for the proposed method, but the hyperparameters were set to: learning rate $\eta = 0.001$, epochs $T = 3000$, and a batch size of 10.

Figure 1 shows the evolution of acceptance rates between adjacent replicas during the optimization steps for both (a) the policy gradient method and (b) the proposed method. While the acceptance rates for the policy gradient method failed to converge to a single value even after 3000 epochs, the proposed method demonstrated rapid convergence, with the initially dispersed rates smoothly approaching a unified value as the optimization progresses. Unlike the optimization using gradient $\nabla_{\beta} f_{\text{uni}}$, which is prone to instability due to unconstrained updates (see Appendix A), our method using the $\log \Delta \beta$ reparameterization successfully avoids such instability.

The stability of our method stems from the global dependency introduced by the variable transformation. Since each inverse temperature is defined as a cumulative sum of intervals, $\beta_j = \beta_1 + \sum_{n=1}^{j-1} \Delta \beta_n$, a change

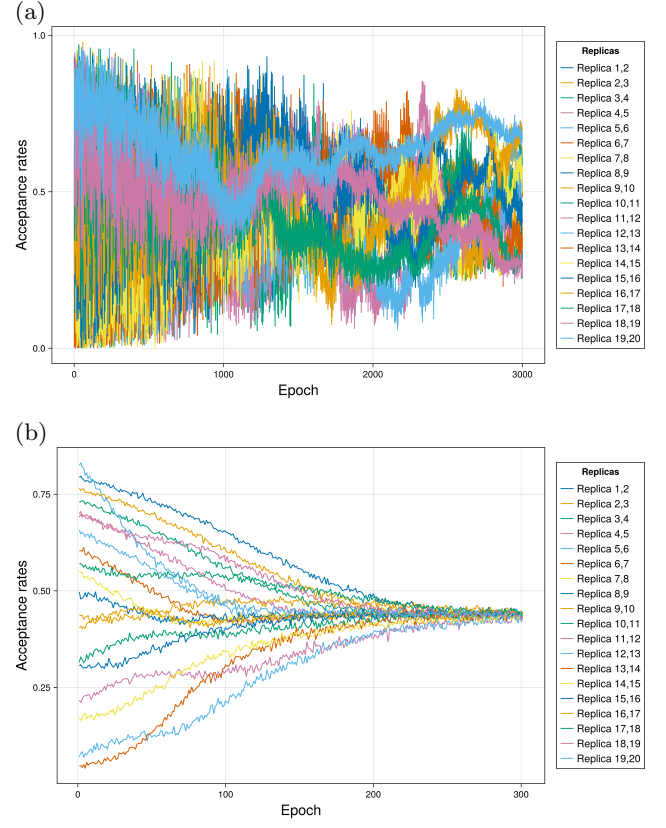


Figure 1: Evolution of acceptance rates between adjacent replicas during the optimization process for the 2D Ising model ($L = 20$). (a) Results using the policy gradient method over 3000 epochs. (b) Results using the proposed method over 300 epochs.

in a single interval parameter L_k shifts the positions of all subsequent replicas $j > k$. This is reflected in the chain rule derived in Eq. (7), where the gradient with respect to L_k becomes a summation of gradients from all subsequent replicas. This means that the update of a local interval is driven not only by its immediate neighbors but by the collective feedback from all replicas at higher inverse temperatures. Therefore, even if the local acceptance rate drops and the gradient $\partial f / \partial \beta_k$ vanishes locally, the non-vanishing gradients from downstream replicas can propagate back to update L_k . This mechanism prevents the optimization from stagnating in plateaus. Consequently, the optimization proceeds robustly without becoming trapped in poor local minima where acceptance rates drop to zero.

Figure 2 shows the learning curves for the policy gradient method and the proposed method. In the policy gradient method, the loss fluctuates within the range of 10^{-2} to 2×10^{-2} after 1000 epochs, failing to show clear convergence. In contrast, the loss of the proposed method decreases sharply within the first 100 epochs and continues to decrease monotonically thereafter, eventually converging to a value below 10^{-3} . This quantitatively demon-

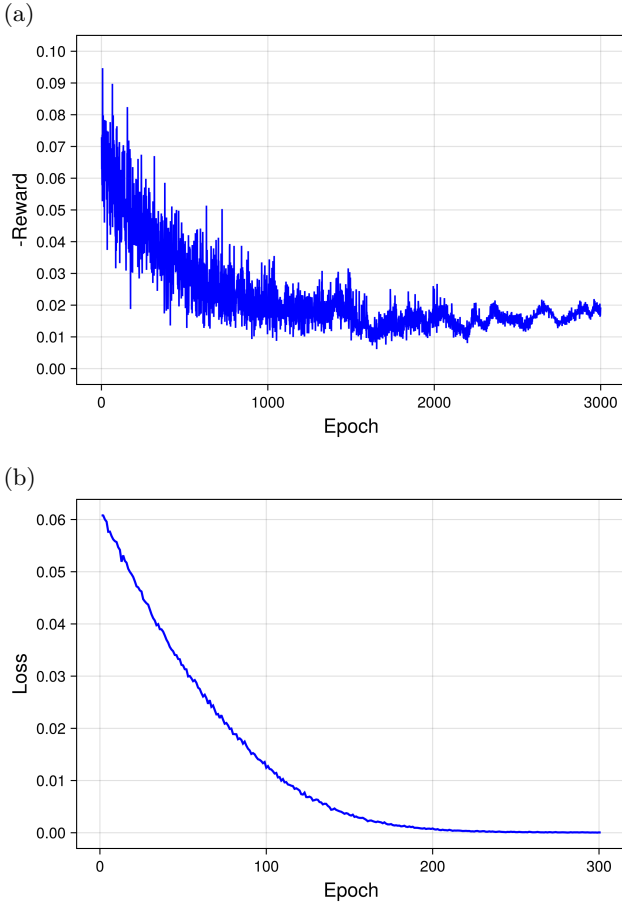


Figure 2: Learning curves for the 2D Ising model ($L = 20$). (a) Policy gradient method: The negative reward equivalent to the loss function is plotted against the epoch. (b) Proposed method: The loss function is plotted against the epoch.

strates that the proposed method successfully achieves its objective of uniform acceptance rates.

We also attempted to optimize the inverse temperature vector using the loss function $f_{\log}(\beta)$ proposed in [20] within our reparameterization framework. Since our problem setting fixes both endpoints β_1 and β_M , the last interval $\Delta\beta_{M-1}$ is determined dependently as $\Delta\beta_{M-1} = (\beta_M - \beta_1) - \sum_{k=1}^{M-2} \Delta\beta_k$. In our experiments, we observed that optimization using f_{\log} was highly unstable, similar to the results for protein folding [20]. Specifically, the gradients derived from the logarithmic metric aggressively expanded certain intervals, causing the sum of the first $M - 2$ intervals to exceed the total range $\beta_M - \beta_1$. This resulted in a violation of the boundary constraint $\Delta\beta_{M-1} \geq 0$, leading to a simulation failure. Therefore, we conclude that the variance-based approach offers superior stability for constrained temperature optimization in discrete spin systems compared to the logarithmic metric.

Figure 3 shows the optimization process of the inverse

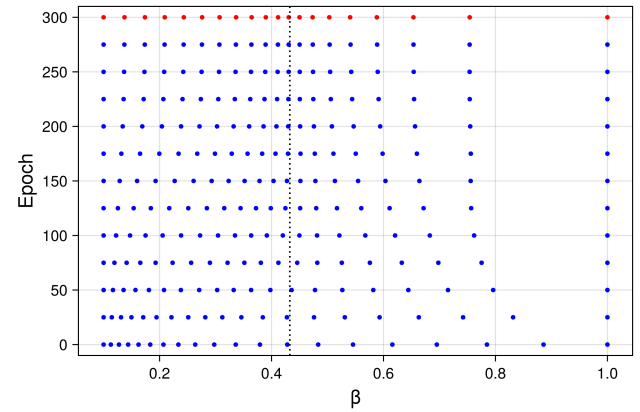


Figure 3: The inverse temperatures at different optimization steps in the 2D Ising model ($L = 20$). Starting from the initial geometric progression (epoch 0), the optimization process progressively concentrates the inverse temperatures around the value indicated by the dashed line, where the specific heat is maximal. The results are shown every 25 steps.

temperatures by the proposed method. The horizontal axis represents the inverse temperature β , and the vertical axis represents the epoch in optimization. In the initial state (epoch 0), the inverse temperatures were arranged in a geometric progression. As the optimization progresses, each temperature point gradually moves, and it is clearly observed that they eventually cluster in the vicinity of the inverse temperature where the specific heat reaches its maximum.

This behavior is plausible in terms of phase transition. Near the critical point, the specific heat exhibits a sharp peak, causing energy fluctuations to become significantly large. To maintain a constant acceptance rate between adjacent replicas, it is necessary to ensure sufficient overlap between their Boltzmann distributions. This requires making the inverse temperature interval $\Delta\beta$ smaller in the region of high specific heat. Our proposed method successfully optimized the temperature intervals to satisfy this physical requirement automatically.

We attribute the primary reason for the failure of the policy gradient method to the fact that the policy assumes independence among the action components. In systems exhibiting phase transitions, such as the 2D Ising model, achieving uniform acceptance rates between adjacent replicas necessitates placing inverse temperatures closely spaced near the critical point and widely spaced in other regions, as suggested by Fig. 3. This implies that the action \mathbf{a} should not be independent but rather exhibit strong correlations across indices to capture such variation in optimal intervals. However, since the policy in [21] is modeled by a multivariate normal distribution with a diagonal covariance matrix $\sigma^2 \mathbf{I}$, it assumes that each interval varies independently. Consequently, during the optimization process, actions significantly distant

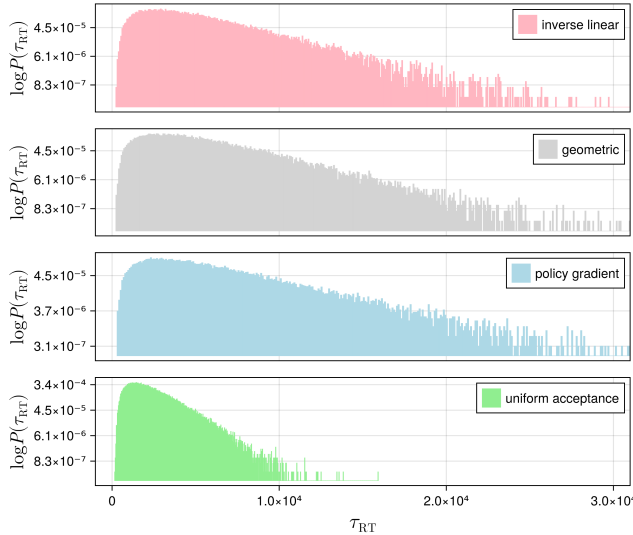


Figure 4: Distribution of round-trip times for the 2D Ising model ($L = 20$) under four different temperature selection strategies: from above, inverse linear, geometric progression, the strategy resulting from the policy gradient method, the proposed strategy. The y-axis is presented on a logarithmic scale. The density is estimated from 10^7 MCS evaluation runs for each strategy.

from the initial policy parameters θ_0 have an extremely low probability of being sampled. As a result, the probability of sampling the optimal parameters becomes significantly low, making it difficult to discover the optimal temperature intervals that require exploration across the wide range of scales induced by the phase transition.

Finally, we evaluated the sampling efficiency using the round-trip time. Figure 4 shows the distribution of round-trip times observed during 10^7 MCS run for each of the four strategies: the proposed method labeled “uniform acceptance”, the policy gradient method, the geometric progression, and the inverse linear. The distributions exhibit a heavy-tailed behavior characterized by a power-law decay. This characteristic indicates that while the distribution peaks at relatively short durations, there is a non-negligible probability of extremely long excursions. Given this long-tailed nature, the mean is highly sensitive to rare, extreme events and may not accurately reflect the typical efficiency. Therefore, we adopted the median instead of the mean for evaluation. Figure 5 provides a quantitative comparison of these distributions using a box plot; outliers have been omitted for clarity. This figure clearly demonstrates the superior performance of the uniform acceptance rates achieved by the proposed method. It achieves the lowest median round-trip time indicated by the center line in the box and also the most compact interquartile range (IQR). Specifically, the proposed method reduced the median round-trip time by 57.7% compared to the geometric progression.

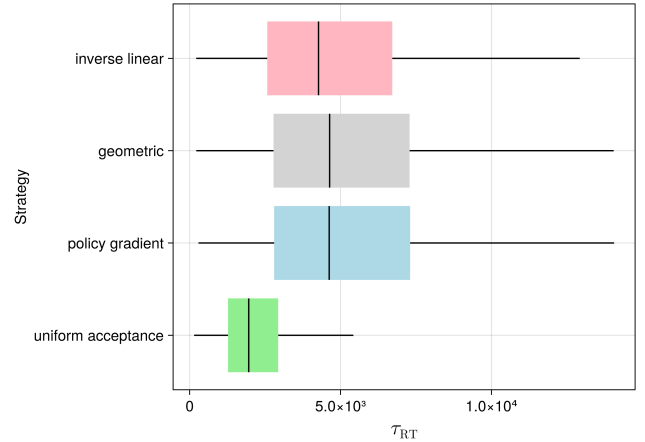


Figure 5: Box plot of the round-trip time distributions for the 2D Ising model ($L = 20$) under four strategies. Outliers, defined as data points falling beyond 1.5 times the IQR from the box, are omitted for clarity.

C. XY Model

The Hamiltonian \mathcal{H}_{XY} for the 2D XY model is given by:

$$\mathcal{H}_{\text{XY}} = -J \sum_{\langle i,j \rangle} \cos(\theta_i - \theta_j), \quad (20)$$

where $\theta_i \in [0, 2\pi)$ represents the angle of the spin vector on site i of a square lattice with $N = L^2$ spins ($i = 1, \dots, N$). The term $\sum_{\langle i,j \rangle}$ denotes the sum over all nearest-neighbor spin pairs. We set the interaction strength $J = 1$.

The 2D XY model is known to exhibit a Berezinskii-Kosterlitz-Thouless (BKT) transition [28–30] at a finite temperature, related to the unbinding of vortex-antivortex pairs. Near the transition temperature, the system exhibits slow dynamics and long correlation lengths, which pose a significant challenge for conventional MCMC sampling. Therefore, optimizing the temperatures for the RXMC method is crucial for efficiently exploring the configuration space around this transition.

In the simulations, we used a system size of $L = 20$ and imposed periodic boundary conditions to suppress finite-size effects. The hyperparameters of the initial inverse temperature vector, the geometric progression, were set to $\beta_1 = 0.5, \beta_M = 1.5$ chosen to fully include the critical region. Furthermore, we set the number of equilibration steps to $N_{\text{eq}} = 10^2$ MCS and the sampling steps to $N_{\text{sam}} = 2 \times 10^4$ MCS.

Unlike the analysis of the Ising model, we do not perform a comparative study with the policy gradient method for this and the subsequent model. The results presented in Sec. IV B clearly demonstrate that the policy gradient method failed to converge. Since this failure suggests a fundamental limitation of the method for

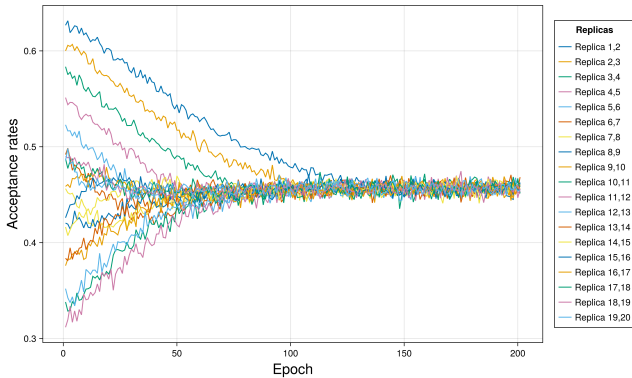


Figure 6: Evolution of acceptance rates between adjacent replicas during the optimization process for the 2D XY model ($L = 20$). Although the optimization was performed for 300 epochs, the results are shown only up to epoch 200 because convergence was already achieved by that point.

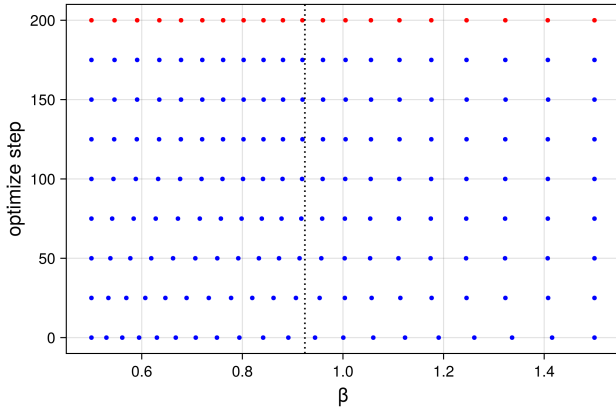


Figure 7: The inverse temperatures at different optimization steps in the 2D XY model ($L = 20$). Starting from the initial geometric progression (epoch 0), the results are shown every 25 steps. The dashed line indicates the approximate inverse temperature where the specific heat peaks.

systems exhibiting phase transitions, applying it to the 2D XY and 3D Edwards-Anderson models is expected to yield similarly poor results. Therefore, we omit these comparisons and focus exclusively on validating the effectiveness and versatility of our proposed method in the remainder of this paper.

Figure 6 shows the evolution of acceptance rates between adjacent replicas. Similar to the Ising model, the initially dispersed acceptance rates rapidly converge to a unified value, demonstrating the effectiveness of the method. Consistent with the Ising model results, the optimization proceeded smoothly without stagnation.

Figure 7 shows the optimization process of the inverse temperatures. Similar to the behavior observed in the

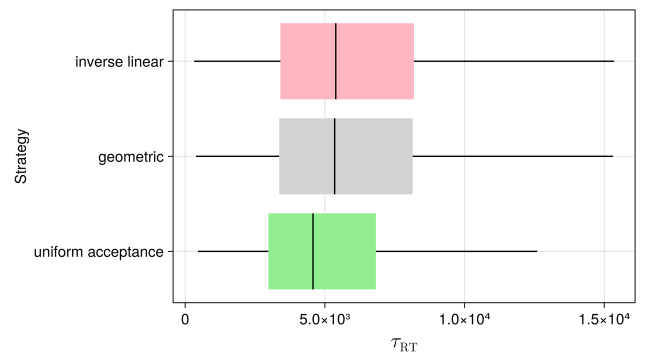


Figure 8: Box plot of the round-trip time distributions for the 2D XY model ($L = 20$) under three strategies, with outliers removed for clarity.

Ising model, the inverse temperatures which started from a geometric progression (epoch 0) autonomously cluster as the optimization progresses. They concentrate in the vicinity of the inverse temperature where the specific heat exhibits its broad peak. This result again confirms the ability of the proposed method to automatically identify the critical region where sampling is most difficult, corroborating the findings from the Ising model.

Figure 8 presents a box plot comparing the round-trip time distributions for the uniform acceptance rates achieved by the proposed method against the geometric progression and inverse linear strategies. Consistent with the Ising model results, the proposed method achieved the lowest median round-trip time and the most compact IQR. Specifically, the proposed method reduced the median round-trip time by 14.5% compared to the geometric progression. This result is particularly significant as it demonstrates that our proposed method is effective not only for discrete spin systems like the Ising model but also for continuous variable systems like the XY model. This successful application to a system with continuous degrees of freedom highlights the versatility and robustness of the proposed framework, confirming its applicability regardless of whether the state variables are discrete or continuous.

D. Edwards-Anderson Model

Following the verification on ferromagnetic systems, we extend our analysis to the 3D Edwards-Anderson (EA) model [31]. This model serves as a canonical example of spin glasses, allowing us to test the efficacy of the proposed method in a more challenging scenario involving quenched disorder and a complex energy landscape. The Hamiltonian \mathcal{H}_{EA} of the 3D EA model is given by:

$$\mathcal{H}_{\text{EA}} = - \sum_{\langle i,j \rangle} J_{ij} \sigma_i \sigma_j, \quad (21)$$

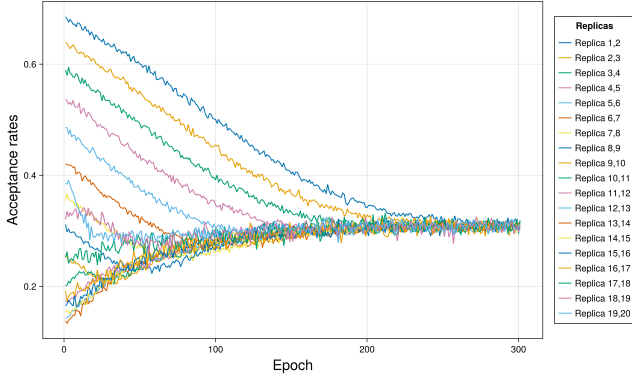


Figure 9: Evolution of acceptance rates between adjacent replicas during the optimization process for the 3D EA model ($L = 8$).

where $\sigma_i \in \{\pm 1\}$ represents an Ising spin on a cubic lattice with $N = L^3$ spins ($i = 1, \dots, N$). The sum $\sum_{\langle i,j \rangle}$ runs over all nearest-neighbor pairs. The interactions J_{ij} are quenched random variables drawn independently from a Gaussian distribution with zero mean and unit variance.

The sampling efficiency of the RXMC method becomes critically dependent on the temperatures for this model, especially near the spin-glass transition point where the specific heat diverges. This divergence causes a significant reduction in the overlap between the Boltzmann distributions of adjacent replicas, creating a critical bottleneck. Thus, careful optimization of the temperatures is essential for overcoming this bottleneck and ensuring an efficient random walk in the temperature space.

In the simulations, we used a system size of $L = 8$ and imposed periodic boundary conditions. The hyperparameters of the initial inverse temperature vector, the geometric progression, were set to $\beta_1 = 0.1, \beta_M = 1.5$ chosen to fully include the critical region. Furthermore, we set the number of equilibration steps to $N_{\text{eq}} = 10^2$ MCS and the sampling steps to $N_{\text{sam}} = 2 \times 10^4$ MCS.

Despite the presence of quenched disorder, the proposed method demonstrates robust performance comparable to that observed in ferromagnetic models. As shown in Fig. 9, the initially dispersed acceptance rates converge smoothly to a uniform value. Correspondingly, as shown in Fig. 10, the inverse temperatures autonomously adapt to the temperature dependence of the specific heat, concentrating them near the critical region where the specific heat peaks. This optimization leads to a significant enhancement in sampling efficiency; as illustrated in Fig. 11, the proposed method achieved the lowest median round-trip time and the most compact distribution among the tested strategies. Specifically, it reduced the median round-trip time by 22.4% compared to the geometric progression. These results confirm the efficacy of our gradient-based framework even for spin-glass systems characterized by complex energy landscapes.

In summary, our extensive simulations consistently

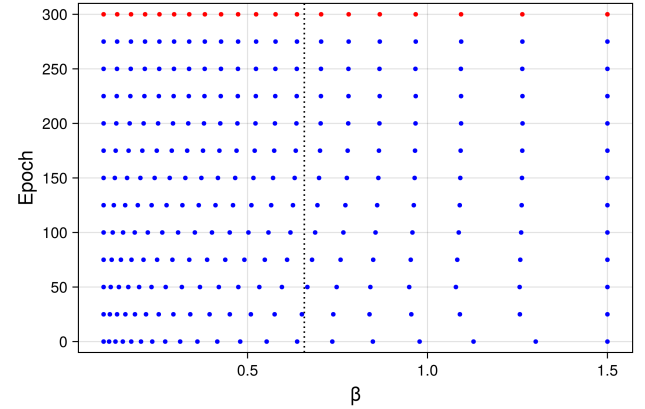


Figure 10: The inverse temperatures at different optimization steps in the 3D EA model ($L = 8$). Starting from the initial geometric progression (epoch 0), the results are shown every 25 steps. The dashed line indicates the approximate inverse temperature where the specific heat is maximal.

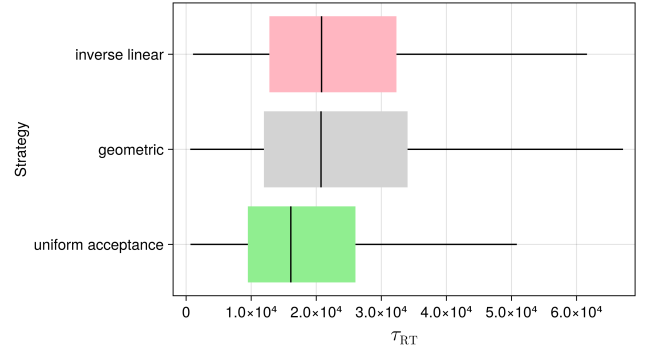


Figure 11: Box plot of the round-trip time distributions for the 3D EA model ($L = 8$) under three strategies, with outliers removed for clarity.

demonstrated the superiority of the proposed method across three benchmark spin systems: the 2D Ising model, the 2D XY model, and the 3D EA model. For every model, the optimization of the inverse temperatures based on uniform acceptance rates led to a significant reduction in round-trip times compared to conventional strategies. These collective results strongly validate the effectiveness and versatility of our gradient-based framework for enhancing the sampling efficiency of the RXMC method, regardless of the system's specific characteristics such as variable type or the presence of disorder.

V. CONCLUSION

In this study, we established a refined online temperature optimization algorithm by extending an existing gradient-based framework [20]. A key feature of our ap-

proach is the introduction of a reparameterization technique that optimizes logarithm of the inverse temperature differences rather than the parameters themselves. This formulation strictly enforces the monotonic ordering of inverse temperatures and fixed boundary constraints, effectively resolving the instability and constraint violations inherent in direct parameter optimization. By defining the loss function as the variance of acceptance rates, our method successfully achieved uniform acceptance rates across the benchmark spin systems, demonstrating superior convergence properties compared to conventional policy gradient methods. Consequently, the optimized temperatures significantly reduced the round-trip times of replicas, directly translating to enhanced sampling efficiency. Furthermore, we confirmed that the method autonomously concentrates temperatures near the critical point where the specific heat peaks, thereby adapting to the characteristics of the system without requiring manual tuning or prior knowledge of a model.

Regarding the application to disordered systems, it should be noted that the optimization in this simulation was performed for a single instance of quenched interactions. For spin glasses, however, significant sample-to-sample variations are known to exist, and optimization on a single instance may not be optimal for others. Applying our method directly would require re-optimization for every new instance, which is computationally inefficient. A more practical strategy, therefore, would be to generate a common inverse temperature vector [14]. This could be achieved by performing the optimization over multiple different instances and utilizing a single, robust vector derived from the averaged results, such as one based on the average loss function. A detailed investigation of such an instance-averaged optimization approach is left for future work.

Several other important considerations remain. First, regarding the loss function, our comparative analysis highlighted that not all differentiable metrics are suitable for online optimization. Indeed, the logarithmic metric in [20] exhibited significant instability, which complicates the determination of convergence criteria and limits practical reliability. This issue applies generally to any loss function that suffers from high estimation variance or sensitivity to boundary conditions. Therefore, while our gradient-based framework offers flexibility in designing the loss function, the selection of a metric that ensures both statistical stability and reasonability is a critical requirement for successful optimization.

Finally, addressing the scalability of the gradient estimator is a vital direction for future research. The score function method adopted in this study is known to suffer from large variance, which typically increases with the system size. This high variance can potentially destabilize the learning process or necessitate the use of excessively small learning rates, thereby slowing down convergence in large-scale simulations. To mitigate this issue, improvements to the score function estimator itself, such as the implementation of control variates or

advanced baselines, are promising avenues [32]. Alternatively, adopting fundamentally lower-variance estimation techniques, such as the alternative differentiation frameworks discussed in Appendix B, could significantly enhance the method's stability and broaden its applicability to larger and more complex systems.

ACKNOWLEDGEMENTS

The authors would like to thank K. Hukushima and Y. Nishikawa for their fruitful discussions and helpful comments. This work is partly supported by JSPS Grant-in-Aid for Early-Career Scientists Grant Numbers 19K14613 (ST) and 25K21297 (SA).

Appendix A: Optimization Using Gradient $\nabla_{\beta} f$

To demonstrate the necessity of the proposed reparameterization strategy, we conducted a comparative experiment applying gradient descent directly to the inverse temperature vector β without enforcing constraints. In this experiment, the learning rate was set to a conservative value of $\eta = 0.001$ to prevent violations of the monotonic ordering, while all other experimental settings followed those described in Sec. IV B.

Figure 12 illustrates the unstable behavior of this direct optimization approach. Figure 12(a) shows the evolution of acceptance rates between adjacent replicas. Notably, the acceptance rate for the specific pair of replicas 13 and 14 drops to near zero immediately and remains stagnant for over 200 epochs. This stagnation corresponds to the behavior observed in Fig. 12(b), which visualizes the evolution of the inverse temperatures. From the early stage of optimization, a gap appears in the inverse temperatures near the inverse temperature corresponding to the peak specific heat, represented by the dashed line.

This phenomenon highlights a fundamental instability inherent in gradient descent using $\nabla_{\beta} f_{\text{uni}}$. During the initial phase, updates tend to drive the inverse temperatures away from the critical region — decreasing the lower components and increasing the higher ones. Consequently, the intervals between adjacent replicas initially positioned near the critical point are significantly widened, causing the acceptance rate to drop to negligible levels and effectively eliminating the gradient signal necessary for recovery. This leaves the learning process trapped in a plateau, unable to correct the excessive intervals. Although the system eventually managed to escape this plateau around epoch 230 in this specific run due to stochastic fluctuations, such prolonged stagnation renders the method inefficient and unreliable. These results underscore the importance of our proposed reparameterization.

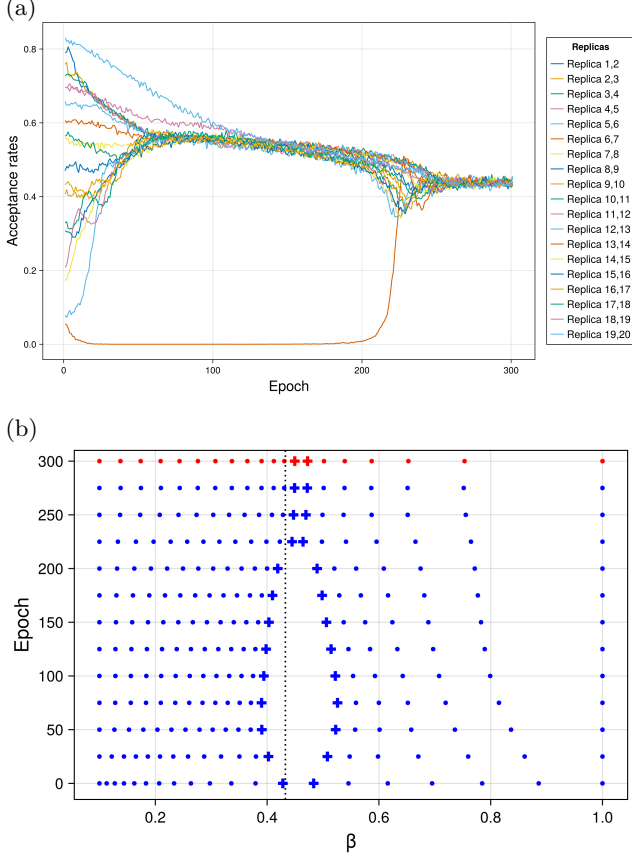


Figure 12: Optimization results using direct gradient descent on $\nabla_{\beta} f$ without constraint enforcement for the 2D Ising model ($L = 20$). (a) Evolution of acceptance rates between adjacent replicas over 300 epochs. The rate for the pair between replicas 13 and 14 drops to zero, causing stagnation for over 200 epochs. (b) Evolution of inverse temperatures. Starting from a geometric progression (epoch 0), snapshots are plotted every 25 steps. The trajectories of the 13th and 14th replicas are distinguished by cross markers to highlight the significant gap emerging between them near the critical point, indicated by the vertical dotted line.

Appendix B: StochasticAD

In this work, we employed the score function method to estimate the gradient of the loss function. As an alternative, we also investigated the use of stochastic automatic differentiation (StochasticAD), another powerful framework for estimating the gradients of expectations, particularly for programs involving discrete random variables [23, 24]. Unlike the log-derivative trick used in the score function method, StochasticAD extends the reparameterization trick [33] to discrete variables by incorporating concepts from finite-difference methods [34]. A key advantage of this approach is that it often yields lower-variance gradient estimators [24].

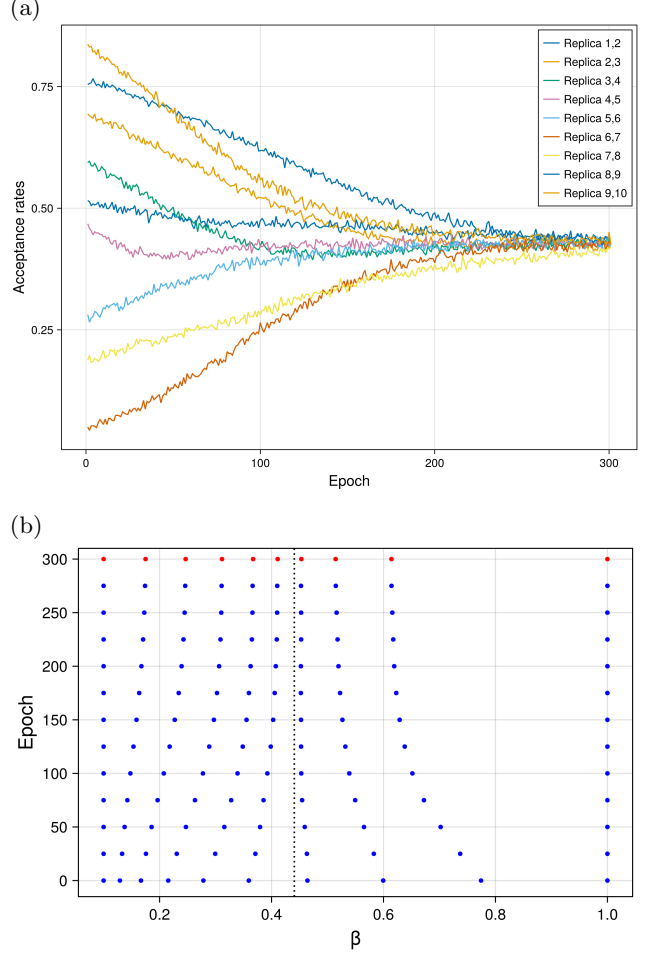


Figure 13: Optimization results using StochasticAD for the 2D Ising model ($L = 10$). (a) Evolution of acceptance rates between adjacent replicas over 300 epochs. The results demonstrate rapid convergence towards a uniform rate across all 9 replica pairs. (b) Evolution of inverse temperatures. Starting from a geometric progression (epoch 0), snapshots are plotted every 25 steps. The dashed line indicates the inverse temperature of maximal specific heat.

To conduct a comparative study, we replaced the gradient estimation module of our framework with StochasticAD, implemented using the `StochasticAD.jl` package in Julia [35]. We then applied this modified framework to the same temperature optimization problem for the 2D Ising model. This experiment was performed on a smaller system with a side length of $L = 10$ and $M = 10$ replicas, while all other hyperparameters, such as the learning rate and optimizer, remained identical to those in the main experiment.

As shown in Fig. 13(a), the StochasticAD-based approach also successfully optimizes the inverse temperature vector, achieving uniform acceptance rates. Moreover, as illustrated in Fig. 13(b), the final optimized tem-

peratures were qualitatively consistent with the results obtained by the score function method, such as concentrating inverse temperatures near the critical point. However, we observed a significant practical drawback: the computational overhead of StochasticAD was sub-

stantial. The total processing time for the optimization was considerably longer than that of the score function method. This computational cost presents a major bottleneck for applying this method to larger system sizes.

[1] N. Metropolis, A. W. Rosenbluth, M. N. Rosenbluth, A. H. Teller, and E. Teller, Equation of state calculations by fast computing machines, *The Journal of Chemical Physics* **21**, 1087 (1953).

[2] W. K. Hastings, Monte carlo sampling methods using markov chains and their applications, *Biometrika* **57**, 97 (1970).

[3] K. Hukushima and K. Nemoto, Exchange monte carlo method and application to spin glass simulations, *Journal of the Physical Society of Japan* **65**, 1604 (1996).

[4] R. H. Swendsen and J.-S. Wang, Replica monte carlo simulation of spin-glasses, *Phys. Rev. Lett.* **57**, 2607 (1986).

[5] C. J. Geyer, Markov chain monte carlo maximum likelihood, in *Computing Science and Statistics: Proceedings of the 23rd Symposium on the Interface*, edited by E. M. Keramidas (American Statistical Association, New York, 1991) pp. 156–163.

[6] Y. Sugita and Y. Okamoto, Replica-exchange molecular dynamics method for protein folding, *Chemical Physics Letters* **314**, 141 (1999).

[7] C. Predescu, M. Predescu, and C. V. Ciobanu, The incomplete beta function law for parallel tempering sampling of classical canonical systems, *The Journal of Chemical Physics* **120**, 4119–4128 (2004).

[8] K. Hukushima, Domain-wall free energy of spin-glass models: Numerical method and boundary conditions, *Physical Review E* **60**, 3606 (1999).

[9] N. Rathore, M. Chopra, and J. J. de Pablo, Optimal allocation of replicas in parallel tempering simulations, *The Journal of Chemical Physics* **122**, 024111 (2004).

[10] D. Gront and A. Kolinski, Efficient scheme for optimization of parallel tempering monte carlo method, *Journal of Physics: Condensed Matter* **19**, 036225 (2007).

[11] B. Miasojedow, E. Moulines, and M. Vihola, An adaptive parallel tempering algorithm, *Journal of Computational and Graphical Statistics* **22**, 649 (2013).

[12] W. D. Vousden, W. M. Farr, and I. Mandel, Dynamic temperature selection for parallel tempering in markov chain monte carlo simulations, *Monthly Notices of the Royal Astronomical Society* **455**, 1919 (2015).

[13] D. A. Kofke, On the acceptance probability of replica-exchange monte carlo trials, *The Journal of Chemical Physics* **117**, 6911 (2002).

[14] H. G. Katzgraber, S. Trebst, D. A. Huse, and M. Troyer, Feedback-optimized parallel tempering monte carlo, *Journal of Statistical Mechanics: Theory and Experiment* **2006**, P03018 (2006).

[15] W. Nadler and U. H. E. Hansmann, Generalized ensemble and tempering simulations: A unified view, *Phys. Rev. E* **75**, 026109 (2007).

[16] I. Rozada, M. Aramon, J. Machta, and H. G. Katzgraber, Effects of setting temperatures in the parallel tempering monte carlo algorithm, *Phys. Rev. E* **100**, 043311 (2019).

[17] S. Syed, A. Bouchard-Côté, G. Deligiannidis, and A. Doucet, Non-reversible parallel tempering: A scalable highly parallel mcmc scheme, *Journal of the Royal Statistical Society Series B: Statistical Methodology* **84**, 321 (2021).

[18] A. Kone and D. A. Kofke, Selection of temperature intervals for parallel-tempering simulations, *The Journal of Chemical Physics* **122**, 206101 (2005).

[19] R. Denschlag, M. Lingenheil, and P. Tavan, Optimal temperature ladders in replica exchange simulations, *Chemical Physics Letters* **473**, 193 (2009).

[20] J. L. MacCallum, M. I. Muniyat, and K. Gaalswyk, Online optimization of total acceptance in hamiltonian replica exchange simulations, *The Journal of Physical Chemistry B* **122**, 5448 (2018).

[21] D. Zhao and N. S. Pillai, Policy gradients for optimal parallel tempering MCMC, in *ICML 2024 Workshop on Structured Probabilistic Inference & Generative Modeling* (2024).

[22] R. J. Williams, Simple statistical gradient-following algorithms for connectionist reinforcement learning, *Machine Learning* **8**, 229 (1992).

[23] G. Arya, M. Schauer, F. Schäfer, and C. V. Rackauckas, Automatic differentiation of programs with discrete randomness, in *Advances in Neural Information Processing Systems*, edited by A. H. Oh, A. Agarwal, D. Belgrave, and K. Cho (2022).

[24] G. Arya, R. Seyer, F. Schäfer, K. Chandra, A. K. Lew, M. Huot, V. Mansinghka, J. Ragan-Kelley, C. V. Rackauckas, and M. Schauer, Differentiating metropolis-hastings to optimize intractable densities, in *ICML 2023 Workshop on Differentiable Almost Everything: Differentiable Relaxations, Algorithms, Operators, and Simulators* (2023).

[25] R. Hagiwara and S. Takabe, Convergence acceleration of markov chain monte carlo-based gradient descent by deep unfolding, *Journal of the Physical Society of Japan* **93**, 063801 (2024).

[26] W. Nadler and U. H. E. Hansmann, Dynamics and optimal number of replicas in parallel tempering simulations, *Phys. Rev. E* **76**, 065701 (2007).

[27] D. P. Kingma and J. Ba, Adam: A method for stochastic optimization, in *3rd International Conference on Learning Representations, ICLR 2015, San Diego, CA, USA, May 7-9, 2015, Conference Track Proceedings* (2015).

[28] V. L. Berezinskii, Destruction of Long-range Order in One-dimensional and Two-dimensional Systems having a Continuous Symmetry Group I. Classical Systems, *Sov. Phys. JETP* **32**, 493 (1971).

[29] J. M. Kosterlitz and D. J. Thouless, Ordering, metastability and phase transitions in two-dimensional systems, *Journal of Physics C: Solid State Physics* **6**, 1181 (1973).

[30] J. M. Kosterlitz, The critical properties of the two-dimensional xy model, *Journal of Physics C: Solid State Physics* **7**, 1046 (1974).

- [31] S. F. Edwards and P. W. Anderson, Theory of spin glasses, *Journal of Physics F: Metal Physics* **5**, 965 (1975).
- [32] S. Mohamed, M. Rosca, M. Figurnov, and A. Mnih, Monte carlo gradient estimation in machine learning, *J. Mach. Learn. Res.* **21** (2020).
- [33] D. P. Kingma and M. Welling, Auto-Encoding Variational Bayes, in *2nd International Conference on Learning Representations, ICLR 2014, Banff, AB, Canada, April 14-16, 2014, Conference Track Proceedings* (2014).
- [34] S. Asmussen and P. Glynn, *Stochastic Simulation: Algorithms and Analysis*, Stochastic Modelling and Applied Probability (Springer New York, 2007).
- [35] Julia, <https://julialang.org>.